Usage of 3D CAD Software for Verification and Representation of Real Machine Measurements and Results

Ing. Zdeněk Braier[1], Ing. Pavel Šidlof[2], CSc.
and Ing. Pavel Klouček[3], Ph.D.

[1,2,3] VÚTS, a.s., Svárovská 619, Liberec XI-Růžodol I, 460 01, Czech Republic

zdenek.braier@vuts.cz, pavel.sidlof@vuts.cz, pavel.kloucek@vuts.cz

Keywords: complicated machine, 3D CAD simulation, verification and representation, experiment on real machine, measurement

Abstract

Many times the connections and transfers between main, driven and end parts are realized by a complicated transmission system with usage of several transfer structures. The contribution describes a complicated sewing machine, which uses several systems, such as tooth belt mechanisms, four-link mechanism, crank mechanism, cam mechanism, tilting mechanism and system shaft inside the hollow shaft etc. for connection of driving and driven mechanism members. A 3D CAD simulation is used for animation and visualization of expected (ideal) status and for verification and representation the measured results.

Introduction

For reasons of inaccessibility of certain mechanisms (parts) or for their miniature size, it is often not possible to install measuring sensors to the parts. Therefore the movements of these parts are derived from movement measurement of some driving parts of mechanism. The derivation is usually performed by a kinematic or dynamic calculation, but it is advantageous to derivate this form of the movement (stroke) directly from a 3D CAD model of a machine mainly for speed and clarity in some cases. Another beneficial and illustrative way of an unusual use of CAD models for measurement can be a representation of the processed measurement results and their animation. The method requires the use of a sophisticated CAD software for an effective utilization and the data exchange adjustment.

The report shows an example of the method usage for measurement of a relatively complicated real sewing machine. Fig. 1 shows the kinematic schema of machine. One of the main measured results, requested by the customer, was a relative movement of a needle eye 9, a looper 10 and a secondary looper 11 (show at Fig. 2), which affect quality and reliability of the sewing process. The looper is driven by the main shaft 3 through a four-link mechanism 4, from which the movement of the secondary looper is derived by an additional cam mechanism 5. The needle bar 8 is guided by a tilting mechanism 13, which is used for adjustable side bight. The movements of the main shaft 3, the upper (driven) shaft 6, which has irregular motion due to a pulley controlled belt mechanism, the acceleration of the needle bar 8 and the needle bar holder 7, which guides the needle bar, were measured. The measurements were recorded as function of an angular position of the main shaft 3. The data were evaluated in software Wolfram Mathematica. The evaluation of the movement of parts 10, 11, derived from the movement of the shaft 3, was verified by the CAD model. The

evaluated relative movements of the needle eye 9, the looper 10 and the secondary looper 11 were compared with their ideal (theoretical) movements within the CAD models.
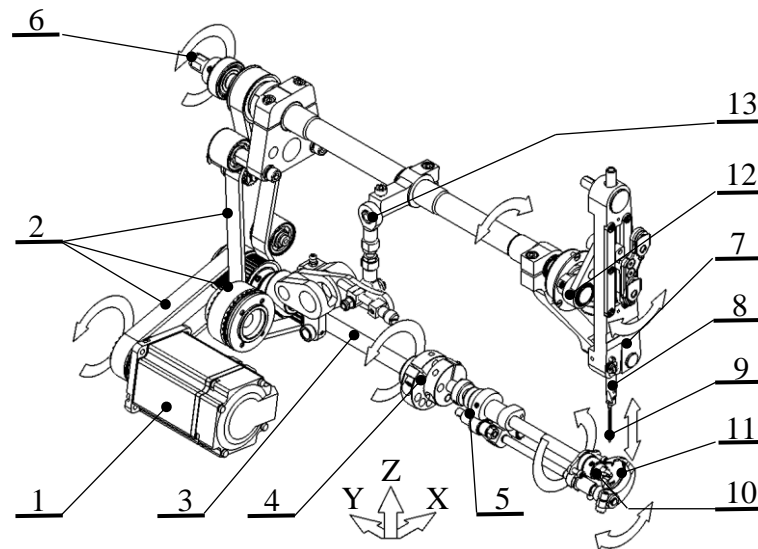
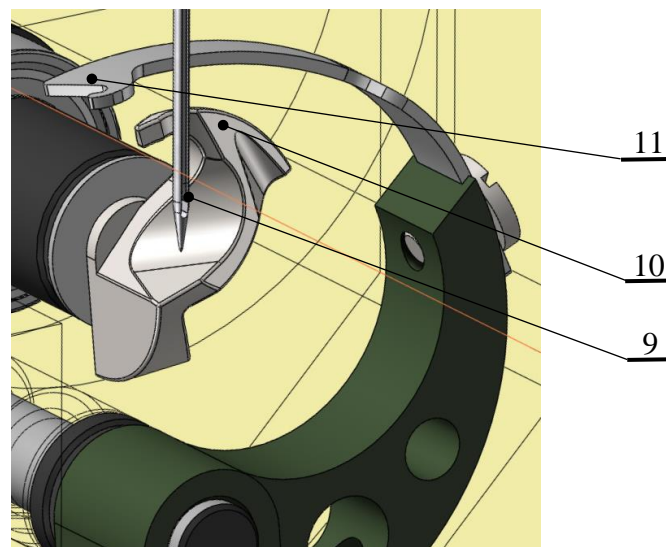

Fig. 1 Kinematic schema of machine

Fig. 2 Detail of needle, looper and secondary looper

Legend of Fig. 1, 2: 1 – servomotor, 2 – belt, 3 – main shaft, 4 – four-link mechanism, 5 – cam mechanism, 6 – upper (driven) shaft, 7 – needle bar holder, 8 – needle bar, 9 – needle (needle eye), 10 – looper, 11 – secondary looper, 12 – crank mechanism of needle bar, 13 – tilting mechanism

Verification and Representation Methods

CAD designers use ideal single parts models for design of ideal (theoretical) CAD models. The CAD models also have ideal mechanical properties. The kinematic connections and movement are generally realized by stiff linkages without clearances. The software, which allow the dynamic calculation of mechanically complicated machines (e.g. Adams, NX), are

hardly accessible for designers due to high cost and the necessity of highly qualified staff. Of course, the calculations by these software are naturally simplified and it is necessary to take measurements. The CAD models may enable the control of measurements, visual presentation of results and animation.

The measured sewing machine has a complex dynamic behavior. There are mechanisms with toothed belts, which have relatively low stiffness. The belt mechanism of the upper shaft is controlled by a tilting mechanism of the needle bar so that during one cycle the rollers vary the lengths of the two branches of the belt and thus modify the angular velocity of the crank shaft and the needle bar movement. The drive of the upper shaft has a considerable influence on the unevenness of the main shaft angular velocity, which influences the looper and secondary looper. In front of the looper, the inserted four-link mechanism significantly changes the looper angular velocity during the cycle. The secondary looper controlled by a cam mechanism performs oscillating movement. The angle and angular velocity of the secondary looper are measured directly by an incremental rotary encoder (IRC). Fig. 3 presents the photos of the machine with the IRC sensor at the main shaft, the upper (driven) shaft (Fig. 3a) and the secondary looper shaft (Fig. 3c). The acceleration sensors positions at the needle bar and the needle bar holder are shown in Fig. 3b. One cannot easily put a sensor on the looper. Because looper drive by the main shaft is relatively stiff, the angle, angular velocity and acceleration of the looper were calculated from the measured angle and angular velocity of the main shaft. The CAD model of the machine was used to check the calculation and correct an initial point of the adjustable looper. Similarly, movement of the needle bar was calculated and checked from the measured movement of the upper (driven) shaft and the needle bar holder.

All variables were simultaneously recorded by a multi-channel Dewetron system that included a special DMU device (a VÚTS system that uses IRC sensors for dynamic measurements of angle, angular velocity and acceleration) enabling angle based records. The calculated speed and acceleration of mentioned parts were calculated from the measured main shaft angle and angular velocity as a time differential.
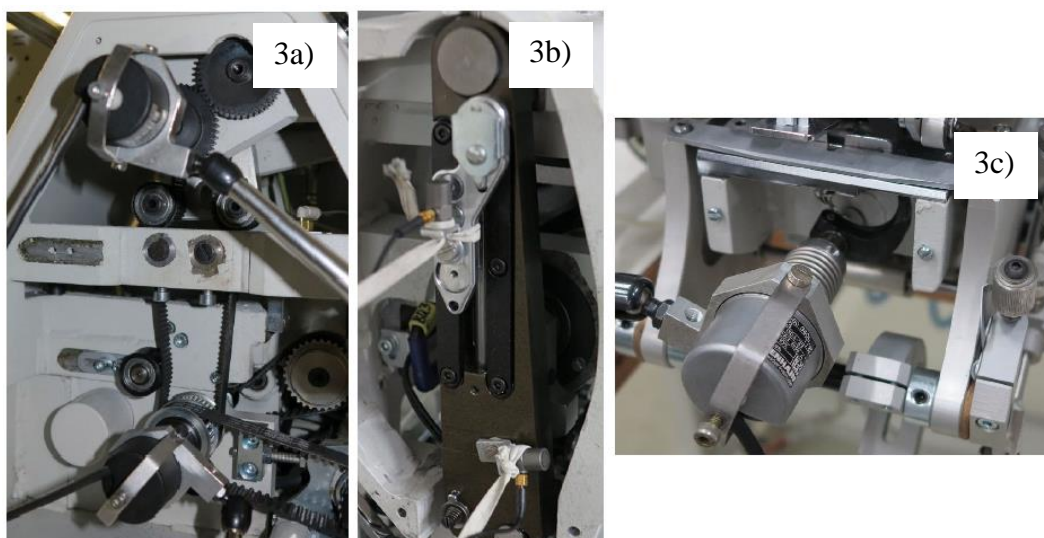

Fig. 3 Photo of real parts with IRC resp. acceleration sensors settings

Results

Fig. 4 shows the simulation of 3D CAD models in SolidWorks. The simulation shows ideal position of the needle, the looper and the secondary looper in XZ-plane as a function of the main shaft angle from 90° to 280° and from 450° to 640° (second half of the cycle). The figure marked 180° and 540° expresses the lowest dead center of the needle eye and start point of the needle motion upwards (reverse). In range from 90° to 180° the needle moves down.
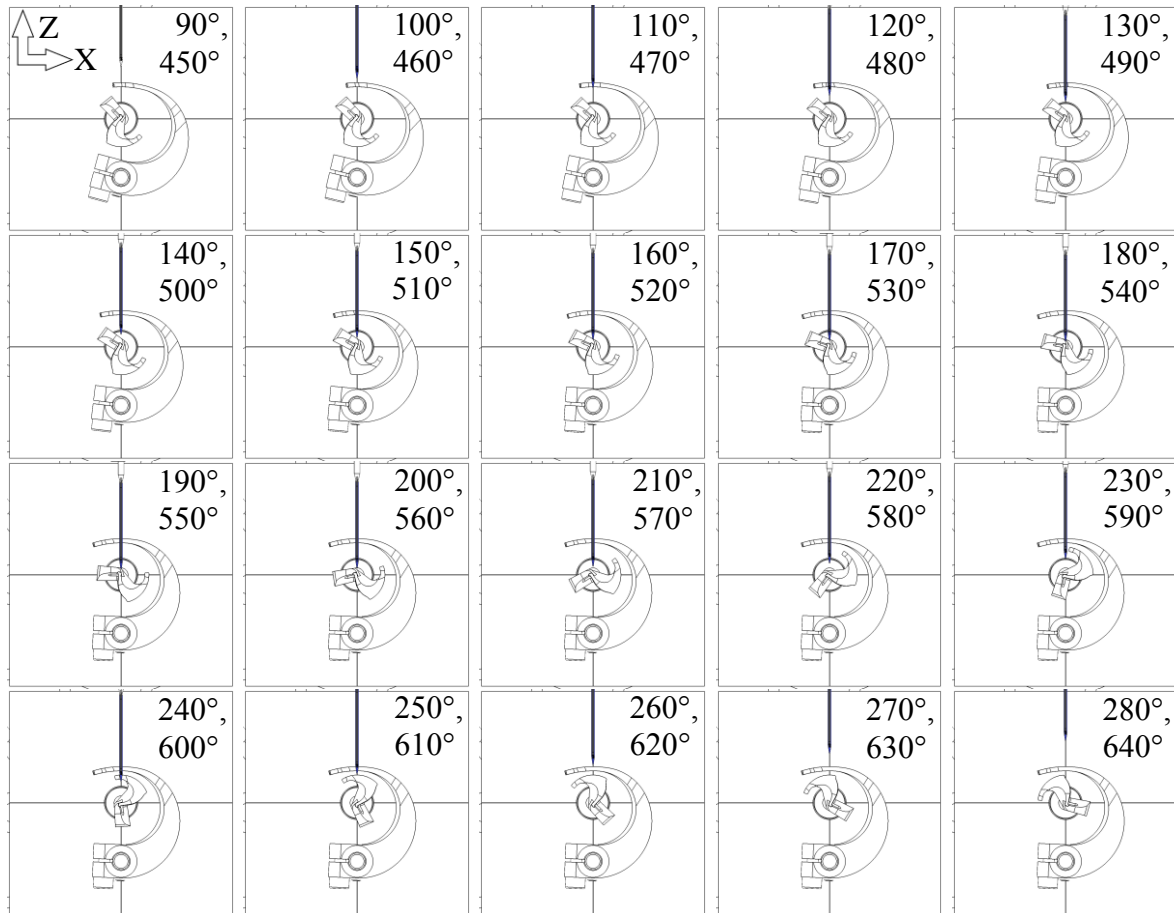

Fig. 4 Ideal needle eye, looper and secondary looper positions without side bight, XZ-plane, 3D CAD models simulation

Fig. 5 shows the mean measured angle of the needle bar tilting without side bight for speeds {1000, 1201, 1401, 1600, 1800, 1899, 1999} [RPM], color marked from green (lowest speed) to red (highest speed). Particular diagrams are mutually shifted by 1 for better clarity, the maximal and minimal values with respect to speed are {{0.05, -0.05}, {0.07, -0.11}, {0.11, -0.16}, {0.13, -0.22}, {0.25, -0.25}, {0.39, -0.33}, {0.45, -0.38}} [deg]. Fig. 6 shows the corresponding mean angular velocity, the diagrams are mutually shifted by 100, the maximal and minimal values are {{3, -4}, {9, -10}, {22, -24}, {26, -26}, {42, -36}, {62, -49}, {66, -56}} [RPM]. Fig. 7 shows the corresponding mean angular acceleration, the diagrams are mutually shifted by 2000, the maximal and minimal values are {{101, -74}, {263, -194}, {496, -567}, {634, -714}, {1179, -1118}, {1560, -1750}, {1872, -1936}} [rad/s^2].
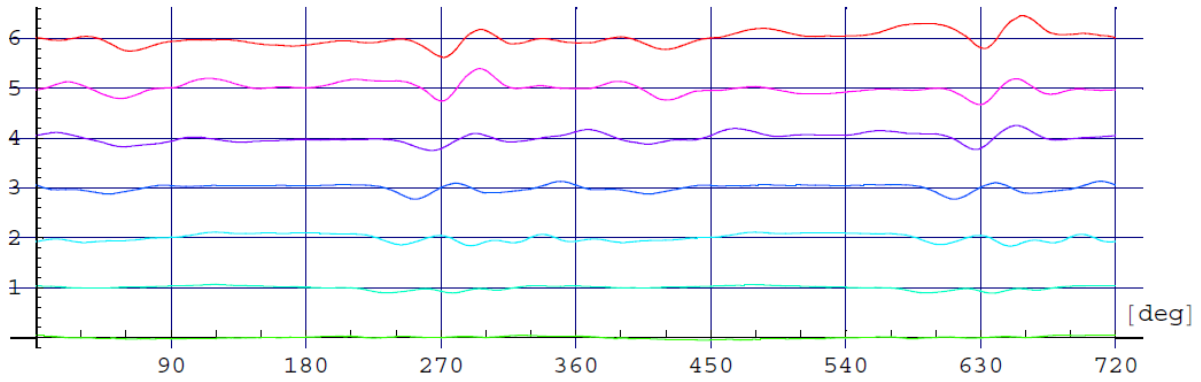
Fig. 5 Mean angle of the needle bar tilting without side bight [deg] vs. main shaft angular position
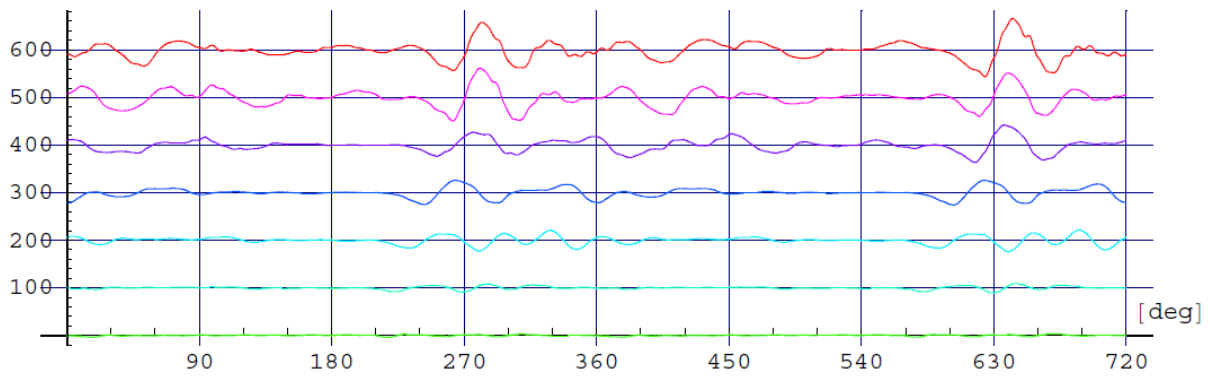

Fig. 6 Mean angular velocity of the needle bar tilting without side bight [RPM] vs. main shaft angular position
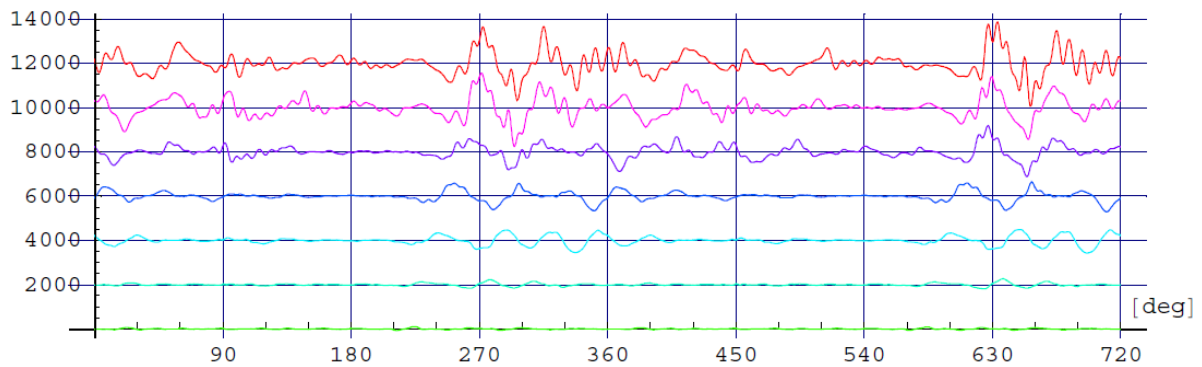

Fig. 7 Mean angular acceleration of the needle bar tilting without side bight [rad/s^2] vs. main shaft angular position

Figures 8 and 9 show the corresponding mean velocity and mean acceleration of the looper, which were modulated by transformation of the four-link mechanism. Fig. 8 shows the mean angular velocity of the looper, the diagrams are mutually shifted by 1000, the maximal and minimal values are {{2176, 266}, {2572, 317}, {2973, 373}, {3336, 427}, {3652, 466}, {3938, 490}, {4146, 523}} [RPM]. Fig. 9 shows the mean angular acceleration, the diagrams are mutually shifted by 10^5, maximal and minimal values are {{23870, -13260}, {34520, -22170}, {48870, -38540}, {61810, -56860}, {89060, -75490}, {100060, -98420}, {116640, -113880}} [rad/s^2].
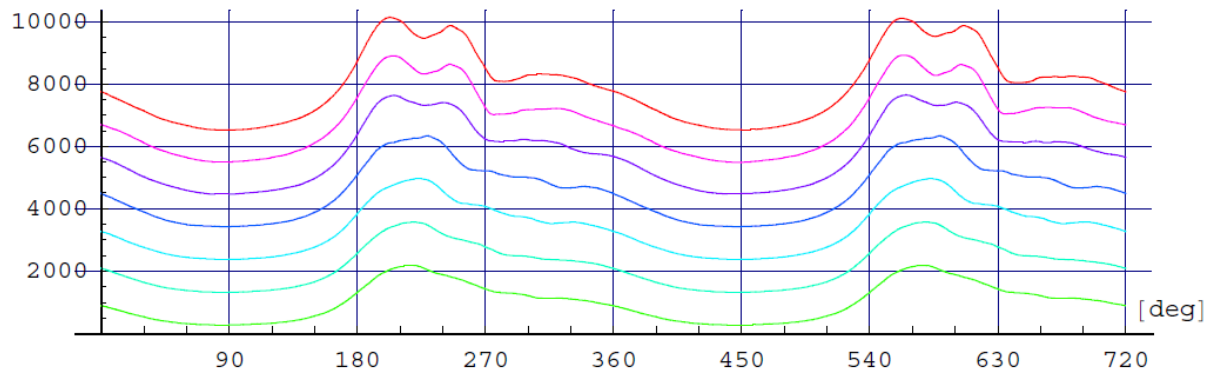
Fig. 8 Mean angle velocity of looper without side bight [RPM] vs. main shaft angular position
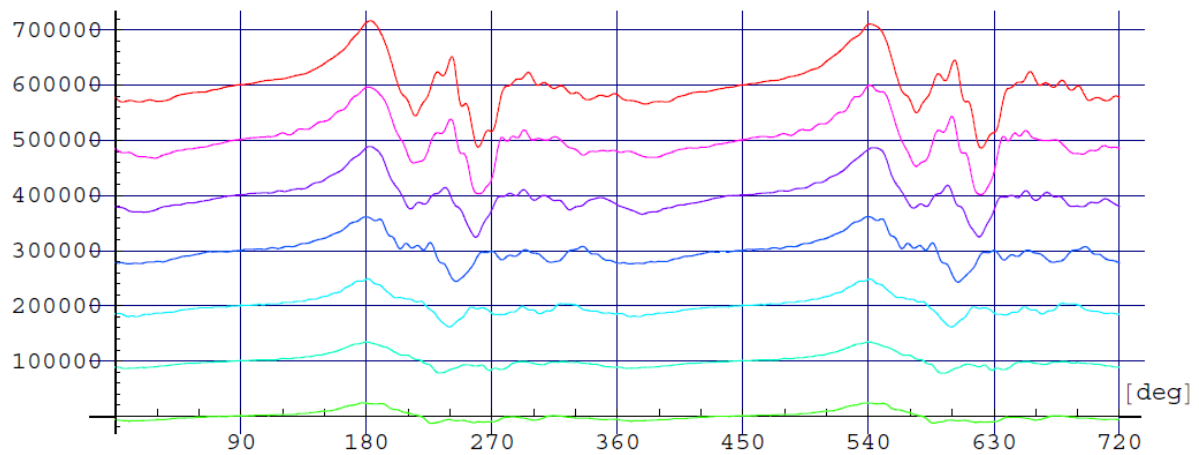

Fig. 9 Mean angular acceleration of looper without side bight [rad/s^2] vs. main shaft angular position

Table 1 links the angles and points of Fig. 4, Fig. 10 and Fig. 11. Angle 180° (event. 540°), highlighted by gray background of cells, expresses the lowest dead center of the needle.

Table 1 Links of the angles and points of figures 4, 10 and 11

Fig. 4	Angle [°]	110, 470	- - -	120, 480	- - -	130, 490	- - -	140, 500	- - -	150, 510	- - -
Fig. 10a	No. [-]	- - -	- - -	1	2	3	4	5	6	7	8
	Angle [°]	- - -	- - -	120	125	130	135	140	145	150	155
Fig. 10b	No. [-]	1	2	3	4	5	6	7	8	9	10
	Angle [°]	470	475	480	485	490	495	500	505	510	515
Fig. 11a	No. [-]	- - -	- - -	- - -	- - -	- - -	- - -	- - -	- - -	- - -	- - -
	Angle [°]	- - -	- - -	- - -	- - -	- - -	- - -	- - -	- - -	- - -	- - -
Fig. 11b	No. [-]	- - -	- - -	- - -	- - -	- - -	- - -	- - -	- - -	- - -	- - -
	Angle [°]	- - -	- - -	- - -	- - -	- - -	- - -	- - -	- - -	- - -	- - -

Fig. 4	Angle [°]	160, 520	- - -	170, 530	- - -	180, 540	- - -	190, 550	- - -	200, 560	- - -
Fig. 10a	No. [-]	9	10	11	12	13	14	15	16	17	18
Fig. 10a	Angle [°]	160	165	170	175	180	185	190	195	200	205
Fig. 10b	No. [-]	11	12	13	14	15	16	17	18	19	20
Fig. 10b	Angle [°]	520	525	530	535	540	545	550	555	560	565
Fig. 11a	No. [-]	- - -	- - -	- - -	- - -	- - -	- - -	- - -	- - -	1	2
Fig. 11a	Angle [°]	- - -	- - -	- - -	- - -	- - -	- - -	- - -	- - -	200	205
Fig. 11b	No. [-]	- - -	- - -	- - -	- - -	- - -	- - -	- - -	- - -	1	2
Fig. 11b	Angle [°]	- - -	- - -	- - -	- - -	- - -	- - -	- - -	- - -	560	565

Fig. 4	Angle [°]	210, 570	- - -	220, 580	- - -	230, 590	- - -	240, 600	- - -	250, 610
Fig. 10a	No. [-]	19	20	21	22	23	24	25	- - -	- - -
Fig. 10a	Angle [°]	210	215	220	225	230	235	240	- - -	- - -
Fig. 10b	No. [-]	21	22	23	24	25	26	27	28	29
Fig. 10b	Angle [°]	570	575	580	585	590	595	600	605	610
Fig. 11a	No. [-]	3	4	5	6	7	8	9	- - -	- - -
Fig. 11a	Angle [°]	210	215	220	225	230	235	240	- - -	- - -
Fig. 11b	No. [-]	3	4	5	6	7	8	9	10	11
Fig. 11b	Angle [°]	570	575	580	585	590	595	600	605	610

Fig. 10 shows the diagrams calculated and evaluated from the measured needle bar acceleration. Fig. 10a) shows the planar detail of the needle eye trajectory without side bight for speed 1600 [RPM], the needle eye vertical coordinate is measured from the looper axes, the main shaft angle range is 120° to 240°, points numbered for 5° steps, X-axis zoomed 10-times. Likewise, Fig. 10b) shows another part of the needle eye trajectory without side bight for the main shaft angle range from 470° to 610° (second part of the cycle). The diagrams show visible influence of vibrations due to the tooth belt connection during the side bight turn-off.
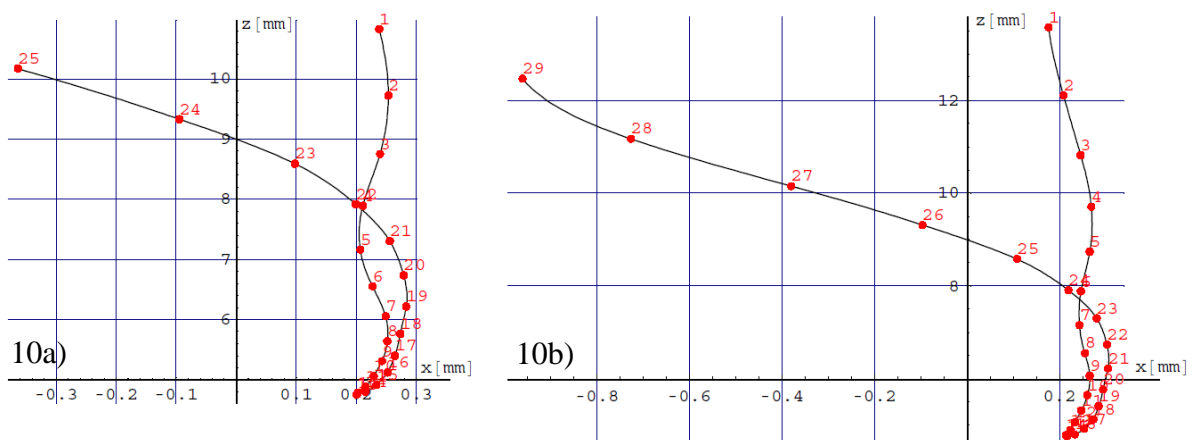

Fig. 10 Needle eye trajectory without side bight, XZ-plane, main shaft angle:
a) 120° to 240°, b) 470° to 610°

Fig. 11 shows the calculated and evaluated results of the looper nose and the needle eye trajectory. Fig. 11a) shows part of the looper nose and the needle eye trajectory without side bight for speed 1600 [RPM] during upwards motion (reverse) of the needle eye, the main shaft angle range is from 200° to 240°, points are numbered for 5° steps. Similarly, Fig. 11b) shows the trajectories for the main shaft angle range from 560° to 610°.
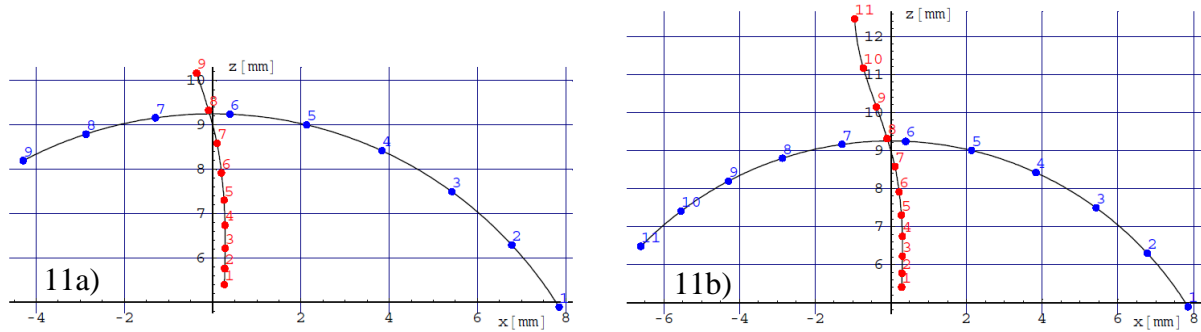

Fig. 11 Looper nose (blue, from right to left) and needle eye (red, upwards) trajectory without side bight, move up (reverse), XZ-plane, main shaft angle: a) 200° to 240°, b) 560° to 610°

Fig. 12 shows the diagrams of the planar detail of the needle eye trajectory with side bight for speed 1600 [RPM]. Fig. 12a) corresponds to the main shaft angle range from 490° to 610° (left stitch), points are numbered for 5° steps, X-axis zoomed 10-times. Similarly, Fig. 12b) shows another part of needle eye trajectory (right stitch), angle range is 120° to 240°, X-axis zoomed equally.
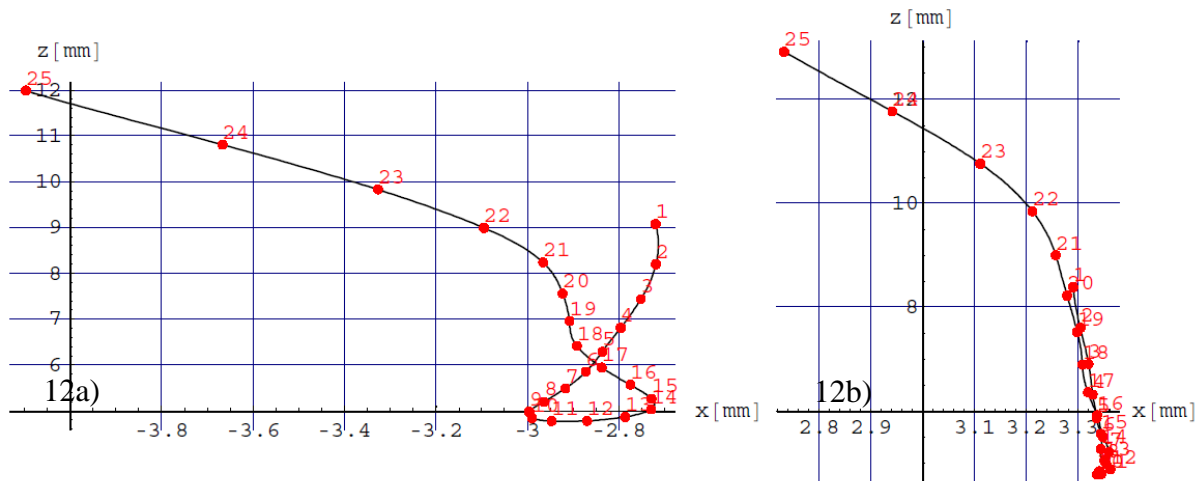

Fig. 12 Needle eye trajectory with side bight, XZ-plane, main shaft angle: a) 490° to 610°, b) 120° to 240°

Fig. 13 shows the calculated and evaluated results of the looper nose and the needle eye trajectory (result of the same measurement). The Fig. 13a) shows trajectories during upwards motion (reverse) of the needle eye, the main shaft angle range is from 560° to 610°, points numbered for 5° steps. Analogously, Fig. 13b) shows trajectories for angle range from 200° to 240°.
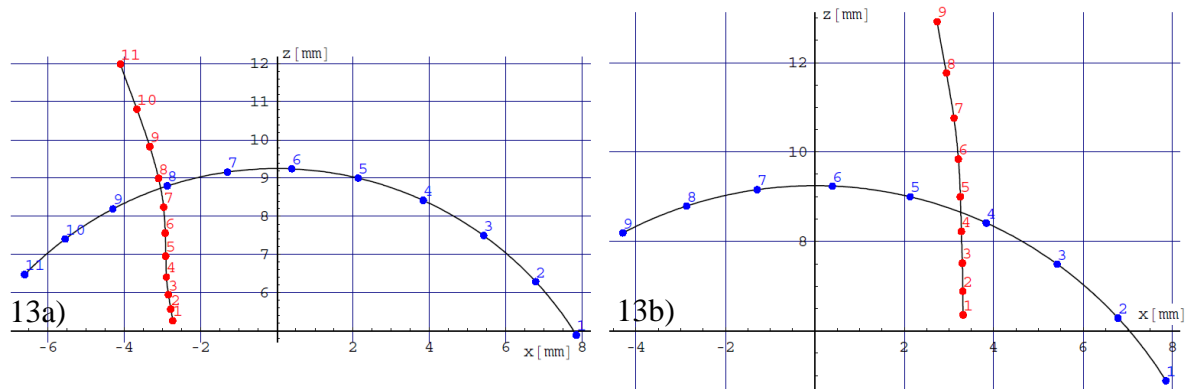
Fig. 13 Looper nose (blue, from right to left) and needle eye (red, upwards) trajectory with side bight, move up (reverse), XZ-plane, main shaft angle: a) 560° to 610°, b) 200° to 240°

The measured results allow us to create animations and visualization of these important movements in the CAD model and assess the reliability of the sewing process and possible errors.

Conclusions

The contribution shows the example of possible common use of the measurement results of a real machine and simulation results of an ideal (theoretical) 3D CAD model. Measurement, verification and simulation of ideal (theoretical) 3D CAD model vs. measurement of real machine is currently being prepared for an expansion to effective usage for other projects from different branches of industry. The CAD models are used to check the measurement results and illustrative animation and visualization of real processes. It is possible to assess not only the correct operation of the machine, but e.g. vibration impact on motion of machine parts by calculating and imaging the corresponding increased displacements superposed to the parts standard motion.

Acknowledgments